

Enhancing Low-Cost Video Editing with Lightweight Adaptors and Temporal-Aware Inversion

Yangfan He^{a*}, Sida Li^{b*}, Kun Li^c, Jianhui Wang^d, Binxu Li^e, Tianyu Shi^f, Jun Yin^g, Miao Zhang^{g†}, Xueqian Wang^g

^aUniversity of Minnesota - Twin Cities, 116 Church St SE, Minneapolis, 55455, Minnesota, USA

^bPeking University, No.5 Yiheyuan Road Haidian District, Beijing, 100871, Beijing, China

^cXiamen University, 422 Siming South Road, Xiamen, 361005, Fujian, China

^dUniversity of Electronic Science and Technology of China, Qingshuihe Campus, 2006 Xiyuan Ave, West Hi-Tech Zone, Chengdu, 611731, Sichuan, China

^eDepartment of Electrical Engineering, Stanford University, 450 Jane Stanford Way, Stanford, 94305, California, USA

^fFaculty of Applied Science & Engineering, University of Toronto, 27 King's College Cir, Toronto, M5S 1A1, Ontario, Canada

^gShenzhen International Graduate School, Tsinghua University, University Town of Shenzhen, Nanshan District, Shenzhen, 518055, Guangdong, China

Abstract

Recent advancements in text-to-image (T2I) generation using diffusion models have enabled cost-effective video-editing applications by leveraging pre-trained models, eliminating the need for resource-intensive training. However, the frame-independence of T2I generation often results in poor temporal consistency. Existing methods address this issue through temporal layer fine-tuning or inference-based temporal propagation, but these approaches suffer from high training costs or limited temporal coherence. To address these challenges, we propose a General and Efficient Adapter (GE-Adapter) that integrates temporal-spatial and semantic consistency with Bilateral DDIM inversion. This framework introduces three key components: (1) Frame-based Temporal Consistency Blocks (FTC Blocks) to capture frame-specific features and enforce smooth inter-frame transitions via temporally-aware loss functions; (2) Channel-dependent Spatial Consistency Blocks (SCD Blocks) employing bilateral filters to enhance spatial coherence by reducing noise and artifacts; and (3) Token-based Semantic Consistency Module (TSC Module) to maintain semantic alignment using shared prompt tokens and frame-specific tokens. Our method significantly improves perceptual quality, text-image alignment, and temporal coherence, as demonstrated on the MSR-VTT dataset. Additionally, it achieves enhanced fidelity and frame-to-frame coherence, offering a practical solution for T2V editing. The project page is https://github.com/codepassionor/Tokenflow_adapter.

Keywords:

Video Edit, Text-to-Video (T2V) Generation, Temporal-spatial Consistency, Semantic Consistency

1. Introduction

Text-to-video (T2V) generation and editing Liu et al. (2024); Wang et al. (2023b); Khachatryan et al. (2023); Bar-Tal et al. (2024); Wu et al. (2023a) aim to create and modify dynamic videos that faithfully interpret textual descriptions, producing visually coherent scenes while ensuring spatial consistency and temporal continuity. Recent advancements in diffusion models have significantly accelerated progress in T2V tasks, enabling more efficient and effective video generation and editing.

Traditional T2V methods rely on large-scale video datasets to learn spatial and temporal dynamics across diverse scenes. Pioneering works such as VideoGPT Yan et al. (2021), CogVideo Hong et al. (2022), and Recipe Wang et al. (2024c)

demonstrate the advantages of leveraging extensive datasets to capture fine-grained motion, object interactions, and scene transitions. However, these methods face significant challenges, including high computational costs, dataset biases, and the need for high-quality annotations.

To address these limitations, early approaches leveraging pre-trained text-to-image (T2I) diffusion models Wang et al. (2024a,b); Huo et al. (2024); Xu et al. (2024) have emerged as a promising alternative due to their lower computational requirements. Notable examples include Animatediff Guo et al. (2023), Tune-A-Video Wu et al. (2023b), and TokenFlow Geyer et al. (2023a), which offer cost-effective solutions while maintaining acceptable performance. These approaches can be broadly categorized into training-based and training-free strategies. Training-based strategies focus on fine-tuning temporal or attention layers to enhance temporal consistency and improve editing performance. While effective, this approach incurs high training costs and limited scalability. To mitigate these issues, adapter-based methods Mou et al. (2023); Balaji et al. (2023); Chen et al. (2023); Feng et al. (2023) have been introduced. These methods integrate temporal or attention layers, reducing training costs and improving generalization. However, their relatively large parameter sizes and limited adaptability highlight the need for

*These authors contributed equally to this work.

†Corresponding author.

Email addresses: he000577@umn.edu (Yangfan He^{a*}), 2200013094@stu.pku.edu.cn (Sida Li^{b*}), swe2209523@xmu.edu.my (Kun Li), 2022091605023@std.uestc.edu.cn (Jianhui Wang), andy0207@stanford.edu (Binxu Li), ty.shi@mail.utoronto.ca (Tianyu Shi), yinj24@mails.tsinghua.edu.cn (Jun Yin), zhangmiao@sz.tsinghua.edu.cn (Miao Zhang^{g†}), wang.xq@sz.tsinghua.edu.cn (Xueqian Wang)

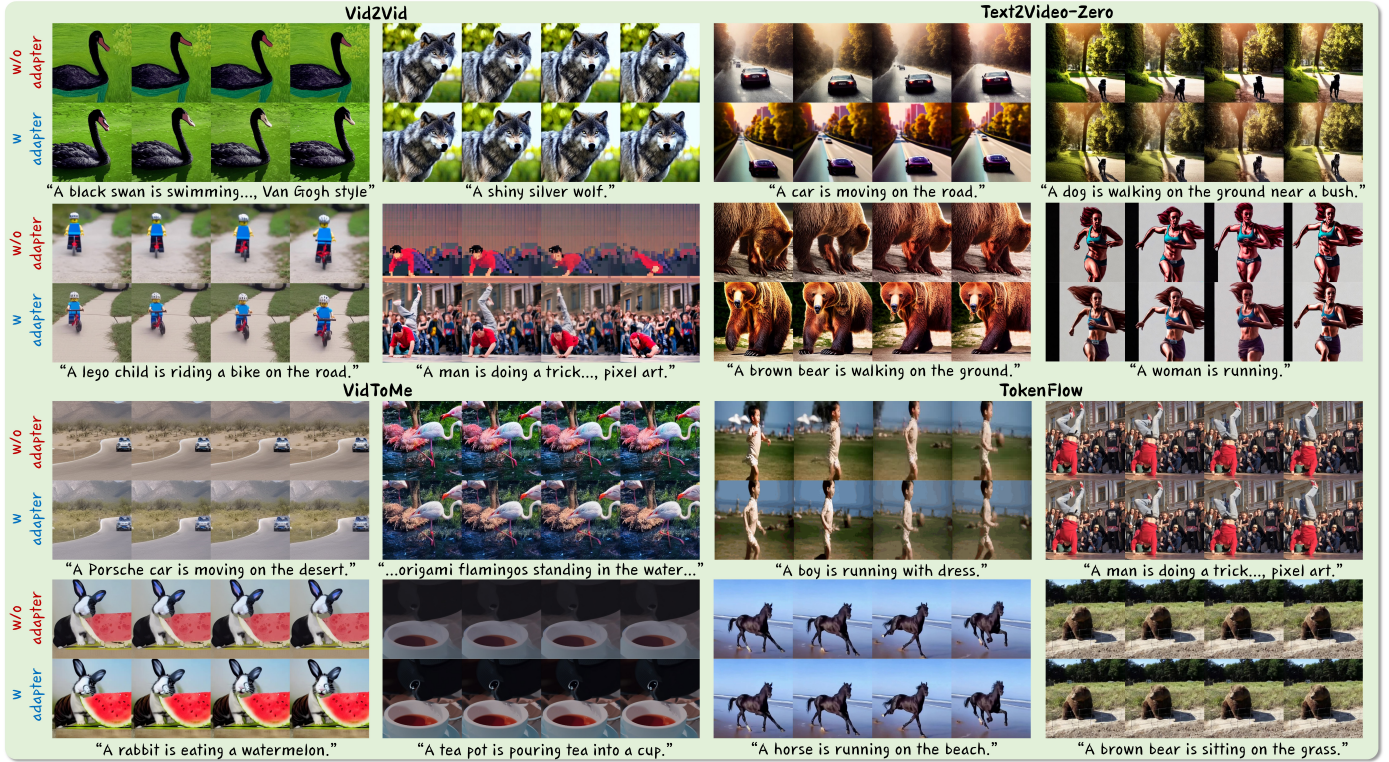


Figure 1: Visual comparison of generated video frames with and without our designed adapter on different algorithms.

further optimization. In contrast, training-free strategies, such as TokenFlow Geyer et al. (2023b), propagate features between neighboring frames during inference, minimizing training costs but often producing outputs of lower quality.

To achieve a balance between computational efficiency and high-quality video generation, we propose a novel Consistency-Adapter Framework. This framework integrates temporal-spatial and semantic consistency while minimizing training expenses. The hierarchical temporal-spatial coherence module (HTC Module) enhances video quality through two key blocks. Frame Similarity-based Temporal Consistency Blocks (FTC Blocks) capture frame-specific information and minimize abrupt feature differences using temporally-aware loss functions. Channel-Dependent Spatially Consistent Blocks (SCD Blocks) employ bilateral filters to reduce noise and artifacts, improving spatial coherence. Lastly, a Token-based Semantic Consistency Module (TSC Module) ensures semantic alignment by leveraging shared prompt tokens for flexible editing and frame-specific tokens to maintain inter-frame consistency.

The main contributions of this paper are as follows:

- We propose a novel plug-and-play consistency-adapter framework that balances computational efficiency and video quality by integrating temporal-spatial and semantic consistency modules.
- We introduce a hierarchical temporal-spatial coherence module (HTC Module) with Frame Similarity-based Temporal Consistency Blocks (FTC Blocks) and Channel-Dependent Spatially Consistent Blocks (SCD Blocks) to ensure spatial and temporal consistency while reducing noise and artifacts.

- We develop a token-based semantic consistency module (TSC Module) that leverages shared and frame-specific tokens to maintain semantic alignment across frames.
- We demonstrate that our lightweight adapter, with only 0.755M trainable parameters for the UNet adapter and 15.4M for the prompt adapter (total size: 860M), achieves over 50% efficiency improvement compared to mainstream T2V models while enhancing temporal consistency, semantic alignment, and video quality.

2. Related Work

Text-to-Video Editing. Text-to-Image (T2I) technology has achieved significant advancements through methods like Generative Adversarial Networks (GANs) Shen et al. (2023a); Karras et al. (2021); Shen et al. (2023b); Karras et al. (2020); Sauer et al. (2022) and diffusion models Shen et al. (2024a); Pan et al. (2018); Soviany et al. (2019); Shen et al. (2023c, 2024b); Gao et al. (2024). However, extending these advancements to Text-to-Video (T2V) remains challenging. Current T2V approaches include inversion and sampling methods, which optimize diffusion processes Rombach et al. (2022); Lu et al. (2022); Shen and Tang (2024); Salimans and Ho (2022); upstream methods, which simplify fine-tuning with adapters Kim and Kim (2024); and downstream methods, which enhance temporal and semantic consistency using complex attention mechanisms.

For example, methods like Gen-L-Video Wang et al. (2023a), FLATTEN Cong et al. (2023), and StableVideo Chai et al. (2023) focus on generating long videos with improved temporal coherence, while approaches like ControlVideo Zhao et al. (2023a)

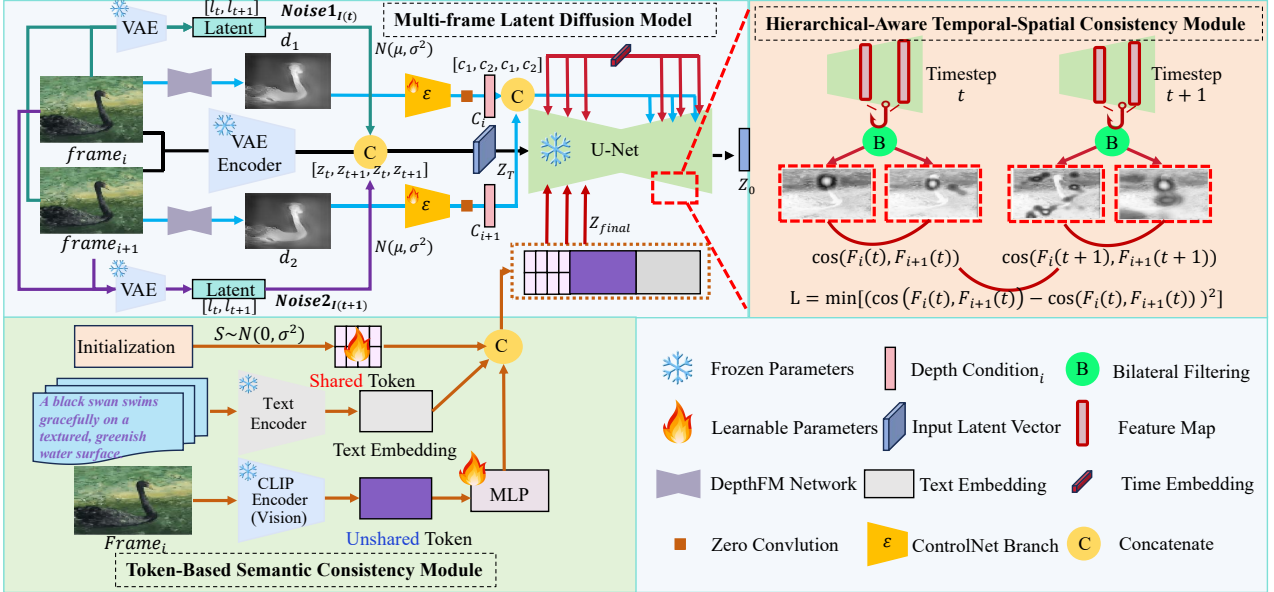


Figure 2: The proposed framework integrates the **Multi-frame Latent Diffusion Model**, **Hierarchical-Aware Temporal-Spatial Consistency Module**, and **Token-Based Semantic Consistency Module**. The top-left illustrates VAE encoding, Gaussian noise injection ($Noise1$, $Noise2$), and latent concatenation for UNet processing. The top-right shows the Temporal-Spatial Consistency Module optimizing frame transitions via temporal loss. The bottom highlights the Semantic Consistency Module combining shared and unshared tokens to enhance semantic alignment and reduce flickering, ensuring both spatial and temporal coherence in video generation.

and MagicProp Yan et al. (2023) aim to enhance the quality of individual video frames. Despite these advancements, existing 2D U-Net-based T2V models often require training from scratch, freezing pre-trained T2I models and relying heavily on complex temporal layers, leading to computational inefficiency and temporal inconsistency. These methods lack a unified, efficient, and lightweight training paradigm that offers strong generalization with a single run and plug-and-play usability.

DDIM Inversion for Enhanced Video Editing. Denoising Diffusion Implicit Models (DDIM) Inversion Song et al. (2022) exploits the reversibility of DDIMs to control latent space content without regenerating the entire image. This technique enables precise adjustments to object shapes, styles, and details while maintaining consistency. Enhancements like EasyInv Zhang et al. (2024) and ReNoise Garibi et al. (2024) refine inversion by iteratively adding and denoising noise, while Eta Inversion Kang et al. (2024) introduces a time- and region-dependent η function to improve editing diversity. MasaCtrl Cao et al. (2023) identifies object layouts by converting images into noise representations, and Portrait Diffusion Liu et al. (2023) merges Q, K, and V values for effective image blending. While these techniques excel in image editing, there remains a lack of optimized DDIM inversion methods tailored for video generation.

Adapters for Video Editing. Initially developed for natural language processing (NLP) Houshy et al. (2019), adapters were introduced to efficiently fine-tune large pre-trained models, as demonstrated in BERT Devlin et al. (2019) and GPT Radford (2018). In computer vision, adapters like ViT-Adapter Chen et al. (2023) enable Vision Transformers (ViT) to handle diverse tasks with minimal fine-tuning. Similarly, ControlNet Zhang et al. (2023) and T2I-Adapter Mou et al. (2023) incorporate lightweight modules for diffusion models to provide additional

control, while Uni-ControlNet Zhao et al. (2023b) reduces fine-tuning costs with multi-scale conditional adapters for localized control. However, current adapters remain limited to specific architectures and lack the flexibility and generalization required for robust video generation tasks.

3. Method

Text-to-video (T2V) editing task models face many challenges, such as maintaining frame-by-frame temporal coherence, ensuring consistent semantics across video frames, and preserving spatial structures throughout the video. To address these challenges, given an input video and text prompts, the text-driven video editing algorithm is designed to produce an edited video that satisfies the following criteria: (1) **Frame Temporal Alignment:** Video editing should ensure temporal coherence among frames by creating smooth transitions between frames and accurately representing motion dynamics as described by the text prompt; (2) **Video Spatial Alignment:** The edited video should ensure that spatial structures and visual content remain consistent across all frames, aligned with the spatial details described in the text prompt while preserving the integrity of the original video’s regions; and (3) **Text-to-video Semantic Alignment:** The algorithm must also ensure that the edited video conveys the intended semantics described in the text prompt while maintaining the contextual consistency of the original video.

To meet the above criteria, we propose a lightweight video adapter designed to enhance temporal-spatial consistency, and semantic consistency, and reduce training costs in text-to-video (T2V) generation using 2D UNet architectures. This adapter integrates multi-frame latent diffusion model 3.1, frame similarity-

based temporal consistency blocks 3.2 to ensure temporal consistency, channel-dependent spatially consistent denoising blocks 3.2 to achieve spatial consistency and smooth noisy latents while minimizing frame artifacts, and a token-based semantic consistency module 3.3 to align the latent semantics of text and video.

3.1. Base Diffusion model

This model differs from traditional methods by directly modeling latent features for consecutive video frames Khachatryan et al. (2023); Qi et al. (2024); Geyer et al. (2023a). By incorporating ControlNet branches, time embeddings, and concatenated latent representations, the model aligns temporal features effectively, reducing flickering and structural inconsistencies. Additionally, the UNet’s decoder layers are optimized for high-resolution outputs, enabling fine-grained reconstruction of temporal dynamics and appearance details. In all, **Multi-frame Latent Diffusion Model** serves as the backbone of our video editing framework, enabling the generation and alignment of video frames through a diffusion process tailored for multi-frame consistency.

The module begins by encoding consecutive video frames ($frame_i$ and $frame_{i+1}$) into latent representations using a Variational Autoencoder (VAE), as shown in Figure 2. These latent encodings (z_t, z_{t+1}) are perturbed with Gaussian noise at each diffusion timestep to simulate noisy latent states ($noise1$ and $noise2$), defined as:

$$z_t \sim \mathcal{N}(\mu, \sigma^2), \quad (1)$$

where μ and σ^2 represent the mean and variance of the Gaussian noise applied.

In this model, **Noise1** and **Noise2** are applied separately to z_t and z_{t+1} to capture frame-specific variations such as lighting, texture, and motion, ensuring that each frame’s unique features are preserved. By injecting independent noise distributions, the model prevents over-smoothing, retaining high-quality spatial details while maintaining temporal consistency. Furthermore, this approach simulates realistic frame-to-frame degradations, enhancing the model’s ability to reconstruct natural and consistent videos during the denoising process.

The latent representations of consecutive frames, z_t and z_{t+1} , along with their noise-injected counterparts, are then combined into a unified latent representation ($[z_t, z_{t+1}, z_t, z_{t+1}]$) to facilitate cross-frame temporal modeling. This concatenated representation captures relationships between frames, enabling the model to jointly process both spatial and temporal features in the latent space. The noisy latent representations are further processed through a UNet-based architecture. To improve temporal coherence across video frames, time embedding vectors are integrated into the UNet. These embeddings encode the timestep information t and help maintain structural consistency during the diffusion process. The latent representations at each timestep are concatenated with control information ($c_t, c_{t+1}, c_t, c_{t+1}$) generated by auxiliary ControlNet branches.

Latent representations for multiple frames are jointly processed through a combination of intermediate feature concatenation, time embedding integration, and latent concatenation.

Temporal feature maps (F_t, F_{t+1}) are concatenated and injected into the UNet, enabling the model to capture inter-frame relationships effectively. Additionally, timestep embeddings encoded within the UNet ensure that the noise schedule aligns with the temporal progression of the video, providing a consistent temporal structure. Furthermore, the concatenated latent representation ($[z_t, z_{t+1}, z_t, z_{t+1}]$) enhances the modeling of spatial-temporal dependencies between frames, significantly reducing flickering and artifacts, and thereby improving overall video quality.

3.2. Hierarchical-Aware Temporal-Spatial Consistency Module

Frame Similarity-based Temporal Consistency Blocks

Diffusion-based video generation methods have advanced significantly in recent years, yet maintaining temporal consistency across video frames remains a critical challenge. Existing models attempt to incorporate temporal dimensionality into the diffusion process using techniques such as pseudo-3D convolutions Singer et al. (2022), sparse-causal attention Wang et al. (2023c), and self-attention feature injection Ceylan et al. (2023). However, these approaches often face drawbacks such as high computational costs, limited scalability, and suboptimal generalization to diverse video content. Unlike previous studies that primarily focus on large-scale retraining or post-hoc temporal smoothing, our approach introduces lightweight blocks with a novel temporal-aware loss function in the UNet’s decoder layers. This method explicitly optimizes the smoothness of transitions between consecutive frames, effectively addressing a key limitation of existing methods. Details about these blocks are provided in Figure 4:

$$x_{t+1} = x_t + \epsilon_t - \theta(x_t, t), \quad (2)$$

where x_t is the image at timestep t , ϵ_t represents predicted noise, and θ denotes the UNet model, which generates static images but lacks temporal relationship modeling; the Temporal UNet Adapter addresses this by integrating lightweight, trainable adapters into the UNet, using hooks to extract intermediate feature maps $\mathbf{F}_{l,b}^t$ from each block (l, b) at timestep t .

$$\mathbf{F}_{l,b}^t = \mathbf{W}_0 \mathbf{x} + \mathbf{B}_{l,b} \mathbf{A}_{l,b} \mathbf{x}, \quad (3)$$

where \mathbf{x} is the input feature, and $\mathbf{B}_{l,b}$ and $\mathbf{A}_{l,b}$ are learnable light-weight low rank matrix parameters. Achieving smooth transitions between video frames requires evaluating the similarity of adjacent feature maps. It is calculated by defining a similarity function:

$$\text{Sim}(\mathbf{F}_t, \mathbf{F}_{t+1}) = \frac{\mathbf{F}_t \cdot \mathbf{F}_{t+1}}{\|\mathbf{F}_t\| \|\mathbf{F}_{t+1}\|}, \quad (4)$$

And \mathbf{x} is the input feature, $\mathbf{B}_{l,b}$ and $\mathbf{A}_{l,b}$ are learnable lightweight low-rank matrix parameters, and smooth transitions between video frames are achieved by evaluating the similarity of adjacent feature maps using a defined similarity function.

$$\mathcal{L}_{\text{temporal}} = \frac{1}{T-1} \sum_{t=1}^{T-1} (\text{Sim}(\mathbf{F}_t, \mathbf{F}_{t+1}) - \text{Sim}(\mathbf{F}_{t-1}, \mathbf{F}_t))^2. \quad (5)$$

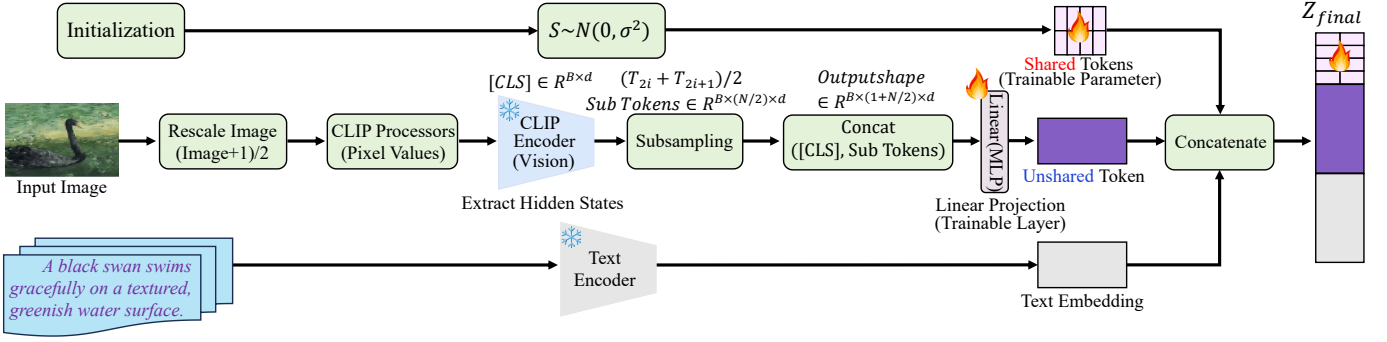


Figure 3: This method combines shared and unshared tokens, maintaining a consistent shared token embedding across timesteps while updating frame-specific unshared tokens to balance global context and local details. Guided by text embeddings, the diffusion model refines noise into semantically consistent images, with frame-dependent unshared tokens introducing per-frame variations in cross-attention guidance and input noise.

Here, T denotes the total number of time steps in the sequence. By minimizing $\mathcal{L}_{\text{temporal}}$, the model aligns the features between consecutive frames, reducing inconsistencies such as flickering and ensuring smoother video transitions. Besides, ensuring smooth and natural transitions during denoising also requires a standard diffusion loss:

$$\mathcal{L}_{\text{diffusion}} = \mathbb{E}_{x_0, \epsilon, t} \left[\|\epsilon - \epsilon_\theta(x_t, t)\|^2 \right], \quad (6)$$

where ϵ represents the noise added to x_0 at time step t , and ϵ_θ is the noise predicted by the model. The overall objective function, which combines the temporal consistency, and diffusion losses, is defined as:

$$\mathcal{L}_{\text{total}} = \lambda_{\text{temporal}} \mathcal{L}_{\text{temporal}} + \lambda_{\text{diffusion}} \mathcal{L}_{\text{diffusion}} \quad (7)$$

where $\lambda_{\text{temporal}}$ and $\lambda_{\text{diffusion}}$ are coefficients set to 1 and 0.01, respectively, to balance the contributions of each loss component. This overall loss helps achieve smooth, temporally consistent video editing.

Channel-Dependent Spatially Consistent Denoising Blocks

Another critical challenge in video editing is the inversion process, which is often necessary for generating edited outputs. Traditional methods like frame-independent DDIM inversion Qian et al. (2024); Wu et al. (2023b); Ren et al. (2024) typically lack video-specific optimization, leading to inconsistencies between frames. To address this, we propose a bilateral filtering DDIM inversion technique that stabilizes latent representations and smooths spatial noisy latents without additional training, significantly improving frame-to-frame spatial consistency and ensuring seamless video generation.

In the context of Denoising Diffusion Implicit Models (DDIM) inversion for video generation, maintaining consistency and quality across consecutive frames is a significant challenge due to noise variations inherent in the diffusion process. The reverse diffusion process, which iteratively denoises a noisy input x_t , follows a probabilistic framework defined by:

$$p_\theta(x_{t-1}|x_t) = \mathcal{N}(x_{t-1}; \mu_\theta(x_t, t), \Sigma_\theta(t)), \quad (8)$$

where $\mu_\theta(x_t, t)$ is the predicted mean, and $\Sigma_\theta(t)$ represents the variance schedule modulating the uncertainty during the reverse step.

Existing DDIM-based video inversion techniques face significant challenges in achieving frame-level smoothness and quality. The stochastic nature of the diffusion process often introduces uneven textures, noise artifacts, and a loss of fine details, leading to visually inconsistent frames. These issues arise from the probabilistic framework of the reverse diffusion process, where the denoising of a noisy input x_t is governed by:

$$x_{t-1} = \frac{1}{\sqrt{\alpha_t}} \left(x_t - \frac{1 - \alpha_t}{\sqrt{1 - \bar{\alpha}_t}} \epsilon_\theta(x_t, t) \right) + \sqrt{1 - \alpha_{t-1}} z, \quad (9)$$

While $\epsilon_\theta(x_t, t)$ predicts the noise, and $\alpha_t, \bar{\alpha}_t$ are scaling factors with z as sampled noise, the process often fails to maintain fine details, leading to perceptual inconsistencies that degrade video quality. Our improved DDIM video inversion algorithm applies **bilateral filtering** to noisy latents x_t , reducing frame artifacts by preserving edges and ensuring a uniform intensity distribution through spatial and intensity-based smoothing:

$$O_x = \frac{\sum_{y \in \mathcal{N}(x)} G_{\text{spatial}}(x, y) G_{\text{intensity}}(I_x, I_y) I_y}{\sum_{y \in \mathcal{N}(x)} G_{\text{spatial}}(x, y) G_{\text{intensity}}(I_x, I_y)}, \quad (10)$$

where $\mathcal{N}(x)$ denotes the neighborhood of pixel x , with y as neighboring pixels contributing to smoothing based on spatial proximity and intensity similarity, defined by their respective intensities I_x and I_y .

$$G_{\text{spatial}}(x, y) = \exp\left(\frac{-(x - y)^2}{2\sigma_{\text{spatial}}^2}\right), \quad (11)$$

$$G_{\text{intensity}}(I_x, I_y) = \exp\left(\frac{-(I_x - I_y)^2}{2\sigma_{\text{intensity}}^2}\right), \quad (12)$$

where σ_{spatial} determines sensitivity to spatial distances, and $\sigma_{\text{intensity}}$ controls the filter's response to intensity differences.

By incorporating bilateral filtering into the DDIM video inversion framework, the noisy latents x_t are smoothed at each timestep, producing refined latents x'_t . The updated DDIM video inversion step is expressed as:

$$x_{t-1} = \frac{1}{\sqrt{\alpha_t}} \left(x'_t - \frac{1 - \alpha_t}{\sqrt{1 - \bar{\alpha}_t}} \epsilon_\theta(x'_t, t) \right) + \sqrt{1 - \alpha_{t-1}} z, \quad (13)$$

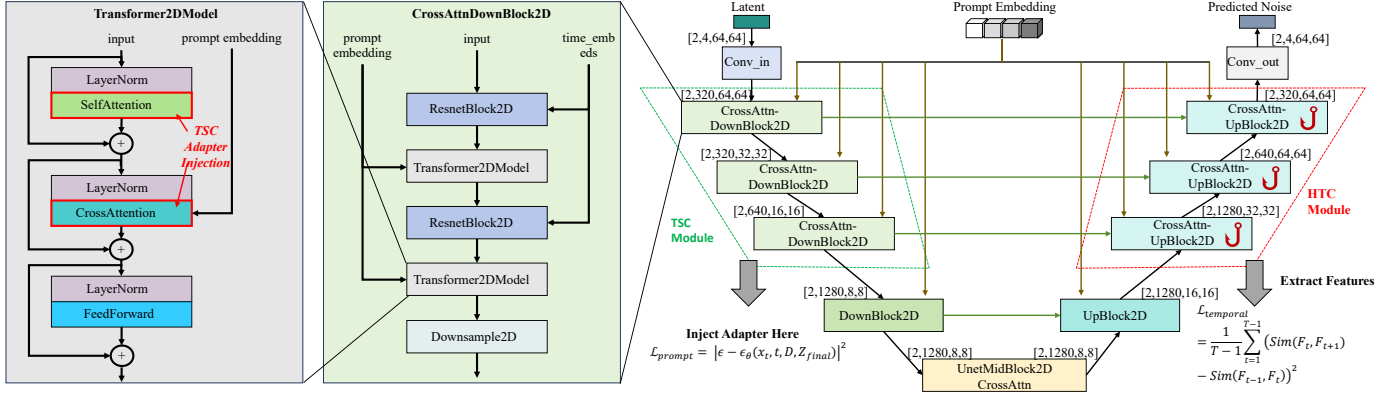


Figure 4: Overview of the UNet framework, illustrating the integration of TSC adapters and HTC modules for temporal coherence and feature extraction. The CrossAttnDownBlock2D and UpBlock2D leverage prompt embeddings and time embeddings, with adapters injected for enhanced prompt conditioning and loss calculations including L_{prompt} and L_{temporal} for robust noise prediction.

where x'_t is the filtered latent obtained from x_t , ensuring smoother and more consistent intensity distributions. By replacing the original noisy latent with x'_t in the reverse diffusion process, the framework aligns denoising dynamics with the smoothed latent distribution. This enhancement effectively reduces noise artifacts, improving overall frame quality throughout the video inversion process.

3.3. Token-Based Semantic Consistency Module

Existing video editing algorithms face significant challenges in aligning video frames with text semantics due to static embeddings and fragmented text integration Singer et al. (2022); Wang et al. (2023c); Ceylan et al. (2023), often resulting in semantic inconsistencies and visual artifacts like flickering. To address this, we propose a Token-Based Semantic Consistency Module that combines shared tokens for global context alignment with dynamic unshared tokens for frame-specific details. The shared tokens ensure that the overarching semantics of the text prompt remain consistent across all frames, maintaining a coherent narrative throughout the video. Meanwhile, the dynamic unshared tokens adapt to frame-specific variations, capturing localized details such as texture, lighting, or motion, which are crucial for preserving temporal continuity. This combination allows our module to balance global coherence with per-frame adaptability, effectively reducing artifacts like flickering and enhancing the overall quality of video editing outputs. The shared token embeddings $T_{\text{share}} \in \mathbb{R}^{N_{\text{share}} \times 768}$ are initialized from a normal distribution $\mathcal{N}(0, 0.02)$, more details see Figure 3. For a given input image I , the CLIP model's vision encoder extracts visual hidden features $H_{\text{vision}} \in \mathbb{R}^{B \times N \times d}$, where B is the batch size, $N = 50$ is the sequence length, and $d = 768$ is the feature dimension. To construct a non-shared subset H_{sub} , adjacent feature vectors along the second dimension are averaged, resulting in $H_{\text{sub}} \in \mathbb{R}^{B \times N/2 \times d}$, defined as:

$$H_{\text{sub}}[:, i, :] = \frac{H_{\text{vision}}[:, 2i, :] + H_{\text{vision}}[:, 2i + 1, :]}{2}, \quad (14)$$

for $i \in \{0, 1, \dots, N/2 - 1\}$.

Next, a projection matrix $W \in \mathbb{R}^{d \times d}$ is applied to H_{sub} to

preserve the feature dimension:

$$Z_{\text{unshare}} = H_{\text{sub}} \cdot W, \quad W = \text{nn.Linear}(d, d). \quad (15)$$

The final text embedding for temporal-aware fine-tuning is constructed as:

$$Z_{\text{final}} = [T_{\text{share}}; Z_{\text{frame}}; C(Z)], \quad (16)$$

where T_{share} represents the shared token embedding, Z_{frame} is the frame-specific unshared token, and $C(Z)$ concatenates conditional and unconditional embeddings along the first sequence dimension. The concatenation is denoted by $[\cdot]$.

During the denoising process, cross-attention provides text guidance by mapping the latent features $X_t \in \mathbb{R}^{M \times d}$ to updated features \tilde{X}_t using the final text embedding $Z_{\text{final}} \in \mathbb{R}^{L \times d}$ as keys and values:

$$Q = W_Q^T X_t, \quad K = W_K^T Z_{\text{final}}, \quad V = W_V^T Z_{\text{final}}, \quad (17)$$

$$\tilde{X}_t = \text{softmax}\left(\frac{QK^T}{\sqrt{d}}\right)V. \quad (18)$$

where $W_Q \in \mathbb{R}^{M \times M}$, $W_K \in \mathbb{R}^{L \times d}$, and $W_V \in \mathbb{R}^{L \times d}$ are the learnable projection matrices for the query, key, and value transformations, respectively.

The updated cross-attention map \tilde{X}_t is integrated into the noise prediction function ϵ_θ to guide the denoising process. The denoising step at timestep t can then be expressed as:

$$x_{t-1} = x_t - \alpha_t \epsilon_\theta(x_t, \tilde{X}_t), \quad (19)$$

where $x_t \in \mathbb{R}^{M \times d}$ (consistent with X_t and \tilde{X}_t) is the noisy latent at step t . The final text embedding Z_{final} integrates shared, frame-specific, and conditional/unconditional embeddings to compute \tilde{X}_t , aligning the denoising operation with frame-specific semantics to ensure global consistency and preserve local details.

During training, the parameters of the CLIP vision encoder (θ) remain frozen, while the adapter parameters, shared embeddings, and projection layers for unshared tokens (ϕ) are optimized iteratively to minimize the following loss function:

$$\text{Loss} = \begin{cases} |\epsilon - \epsilon_\theta(x_t, t, D, Z_{\text{final}})|^2, & \text{for } t \in [0, 0.5T], \\ |\epsilon - \epsilon_\theta(x_t, t, D, Z_{\text{final}})|^2 + \lambda \mathcal{L}_{\text{temporal}}, & \text{for } t \in [0.5T, T] \end{cases} \quad (20)$$



Figure 5: A comparison of video generation quality across different algorithms, with and without the use of an adapter.

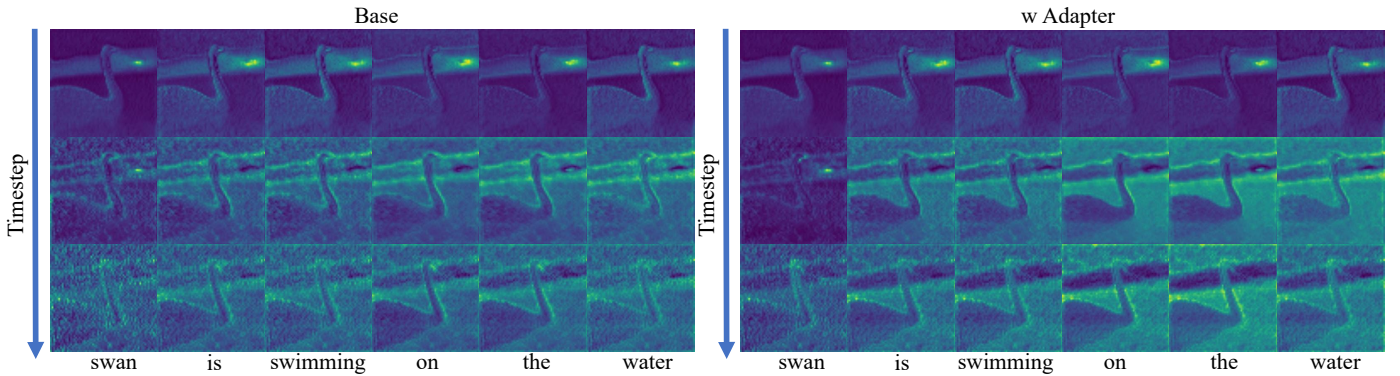


Figure 6: Visualization of attention maps from Unet’s third upsampling block, comparing base and adapter models across 1000 timesteps. The corresponding timesteps from top to bottom are 1, 541, and 981.

where ϵ represents the noise at timestep t , x_t is the input state, and $\mathcal{L}_{\text{temporal aware}}$ is the adjacent frames constraint. The adapter’s parameters are updated as follows:

$$\Theta_{k+1} = \Theta_k - \eta \nabla_{\Theta} \text{Loss}(\Theta_k) \quad (21)$$

With $\Theta = \{\phi_{\text{adapter}}, \phi_{\text{unshared}}, T_{\text{share}}\}$ representing the adapter, unshared token, and shared token embedding parameters, and η as the learning rate, the adapter (ϕ_{adapter}) remains active only

during the extended training interval from 0.5 to 1.0, where it influences $\nabla_{\Theta} \text{Loss}$, otherwise remaining inactive.

4. Experiments

4.1. Implementation Details

We trained a Stable Diffusion v1.5-based model, incorporating an 860M-parameter UNet alongside a 123M-parameter

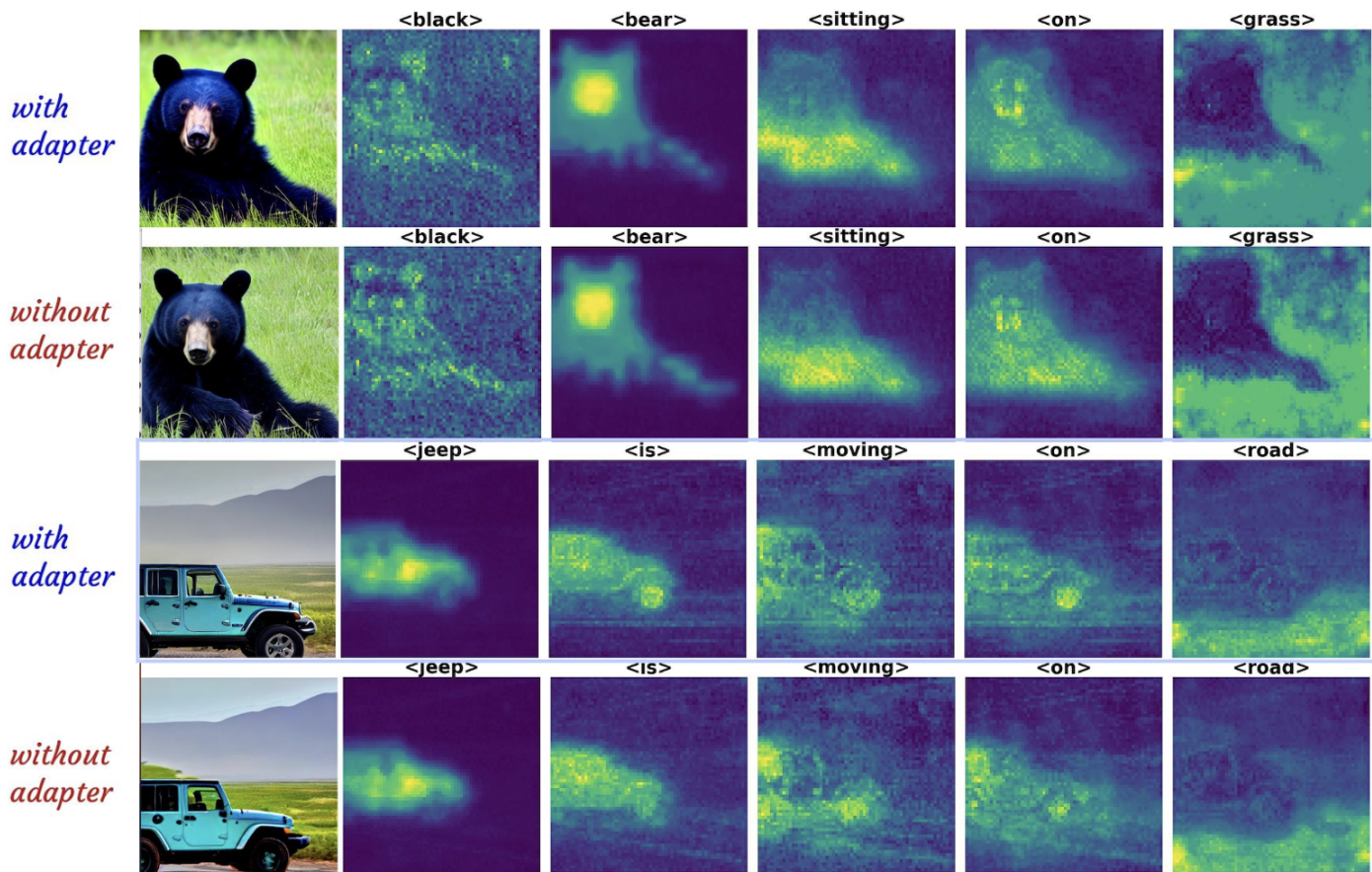


Figure 7: Visualization of attention maps comparing video frames generated with and without the adapter in the Stable Diffusion 1.5 pipeline.

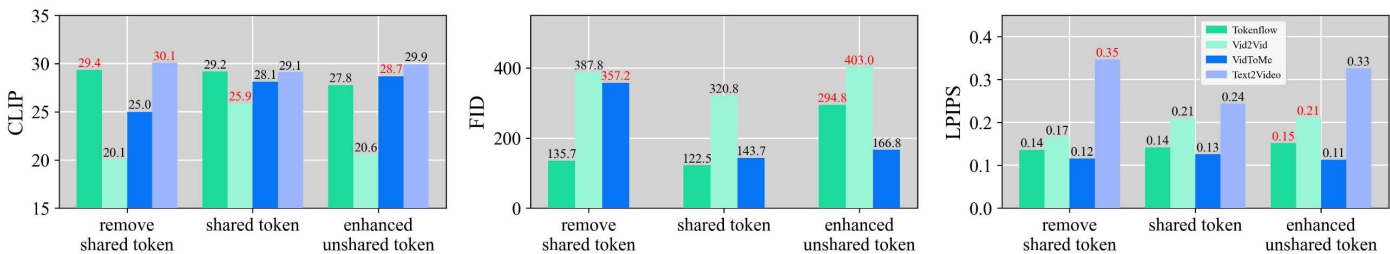


Figure 8: Comparison of token configurations—remove shared, shared, and enhanced unshared—using LPIPS, CLIP, and FID metrics.

text encoder. We integrated a ControlNet designed for depth data, complemented by an adapter featuring a jointly trained PrefixToken module to enhance video-prompt alignment. The training process employed mixed precision (fp16), with a learning rate of $3e-5$, and an input frame resolution of 512×512 . The 1.3G-parameter ControlNet required its dedicated training phase, executed 20 continuous hours with four RTX4090 GPUs. The PrefixToken module itself boasts a modest 2.3M parameters. This module is trained in conjunction with the unet adapter, and joint training needs 18 hours with only one RTX4090 GPU. Training for ControlNet/PrefixToken mirrors the hyperparameters of training above. The training process employs the AdamW optimizer with $\beta_1 = 0.9$ and $\beta_2 = 0.999$ for all of the models. The LoRA update matrix has a dimension of 4. The learning rate is $3e-5$ and the number of warm-up steps in the learning rate

scheduler is 500. The gradient accumulation steps are 8.

UNet adapter. UNet adapter only tunes attentions layer in UNet downsampling block. The adapter parameter size is 860 M. Unet adapter and prompt adapter train together, needs 18 hours with only one RTX4090 GPU.

Prompt adapter. The prompt learner contains a trainable share-token and layers that map image information to tokens. The adapter parameter size is 123 M.

Controlnet. Controlnet initialized from Unet. The model parameter size is 1.3G. It trained on MSRVT dataset for 20 hours with four RTX4090 GPUs.

4.2. Dataset

We used the MSR-VTT dataset, comprising 10,000 video clips across 20 categories with 20 English captions each, for

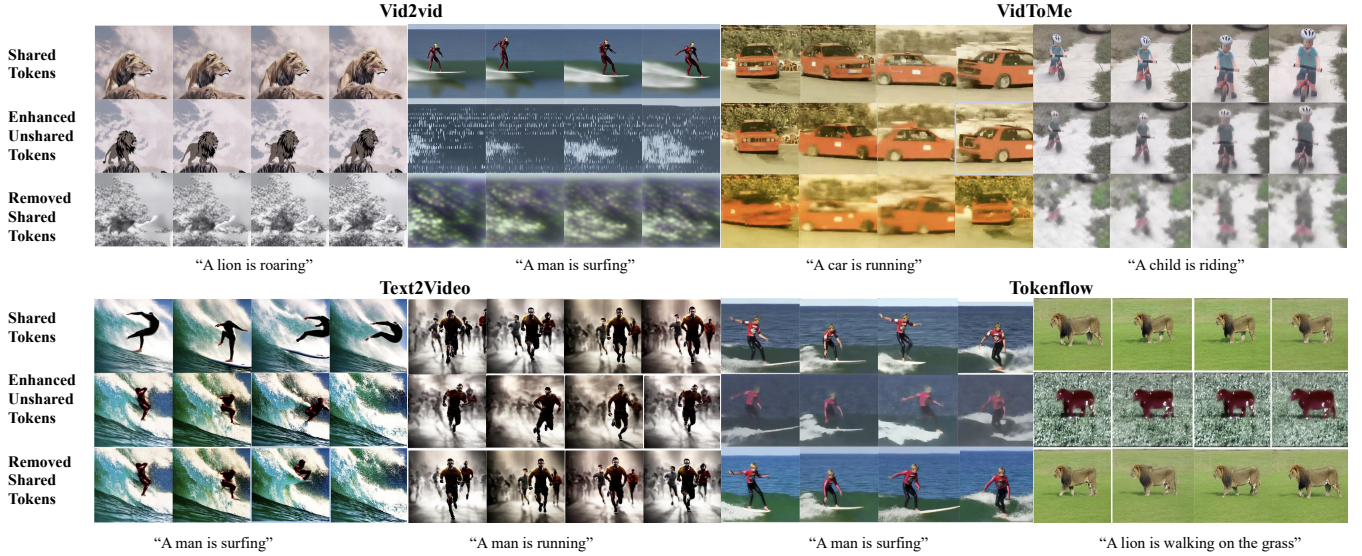


Figure 9: Visualization of video generation models (Vid2Vid, VidToMe, Text2Video, and TokenFlow) using different token strategies: Shared Tokens, Enhanced Unshared Tokens, and Removed Shared Tokens, evaluated across multiple prompts.

Table 1: Comparison of algorithms with and without temporal awareness was conducted using LPIPS, CLIP, and FID metrics on the MSR-VTT Xu et al. (2016) testing set. Adapter parameters were applied during the 0.9-1.0 time intervals of the denoising process. Since text-to-video generation relies solely on textual input without any original source video, there is no FID-based distance between real and generated frames.

Algorithm	Adapter	LPIPS ↓	CLIP ↑	FID ↓
Text2Video-Zero Khachatryan et al. (2023)	✓	0.319	31.38	–
	✗	0.402	28.82	–
TokenFlow Geyer et al. (2023c)	✓	0.129	29.15	143.21
	✗	0.135	28.90	166.72
Vid2Vid Wang et al. (2018)	✓	0.253	32.78	154.30
	✗	0.303	31.94	149.40
VidToMe Li et al. (2023)	✓	0.122	29.94	143.33
	✗	0.123	29.93	146.27

a total of about 29,000 unique words, split into 6,513 training, 497 validation, and 2,990 testing clips. Using the OpenAI ChatGPT API, we modified captions to generate new content, and employed a specialized DataLoader to batch early denoised adjacent frames, converting MP4 videos into WebDataset format for optimized training. During inference, adapter weights were loaded into the StableDiffusionPipeline and integrated into the model at a 50% ratio.

4.3. Quantitative Results

Superior Performance Across Algorithms and Settings

The results in Table 2 demonstrate the versatility and effectiveness of our adapter with a different base diffusion model (SD-XL) and ControlNet conditioning settings. With Canny Edge conditioning, it improves FID from 343.21 to 338.78 and LPIPS from 0.729 to 0.725, enhancing fidelity and perceptual quality. For Human Pose, it boosts CLIP from 29.49 to 33.56, while reducing FID from 365.91 to 362.83 and LPIPS from 0.763 to 0.746, ensuring better semantic alignment. Under Depth Map conditioning, it lowers FID from 343.33 to 339.10, LPIPS from 0.721 to 0.718, and improves CLIP from 29.89 to 31.67, validating the adapter’s ability to enhance visual quality, semantic consistency, and inter-frame coherence across diverse conditions.

Table 2: An ablation study on pretrained ControlNet conditions (controlnet-canny, openpose, depth-sdxl-1.0) with adapter results (yellow) on MSR-VTT human-edited cases for Human Pose demonstrates compatibility and performance gains, with enabled components in green.

Canny Edge	Human Pose	Depth Map	FID ↓	CLIP ↑	LPIPS ↓
✓	✗	✗	343.21 (338.78)	29.15 (31.44)	0.729 (0.725)
✗	✓	✗	365.91 (362.83)	29.49 (33.56)	0.763 (0.746)
✗	✗	✓	343.33 (339.10)	29.89 (31.67)	0.721 (0.718)

Table 1 highlights the compatibility of our adapter with various T2I-based T2V algorithms, showcasing its ability to consistently enhance performance across diverse methods Geyer et al. (2023a); Chu et al. (2024); Li et al. (2023); Khachatryan et al. (2023) with and without adapter injection demonstrates notable improvements in perceptual quality and text-image alignment: Text2Video-Zero achieves smoother transitions and better prompt adherence with LPIPS reduced from **0.402 to 0.319** and CLIP increased from **28.82 to 31.38**; TokenFlow improves motion and texture consistency with a FID drop from **166.72 to 143.21**, alongside LPIPS and CLIP gains; Vid2Vid enhances motion alignment with LPIPS decreasing from **0.303 to 0.253** and CLIP increasing from **31.94 to 32.78**; and VidToMe improves perceptual quality and semantic alignment with LPIPS reduced from **0.126 to 0.114** and CLIP rising from **25.00 to 28.12**, indicating enhanced perceptual quality and semantic alignment.

4.4. Qualitative Results

Figure 5 highlights the pivotal role of the adapter in enhancing video quality across various scenarios and algorithms. In the "lion roaring" example, videos without the adapter suffer from inconsistent facial features and unstable motion across frames, whereas the adapter ensures fluid transitions and a cohesive portrayal of the roaring action. In the "child biking through water" scenario, videos without the adapter exhibit artifacts and temporal inconsistencies, such as distorted water reflections and unnatural motion, which the adapter effectively resolves,

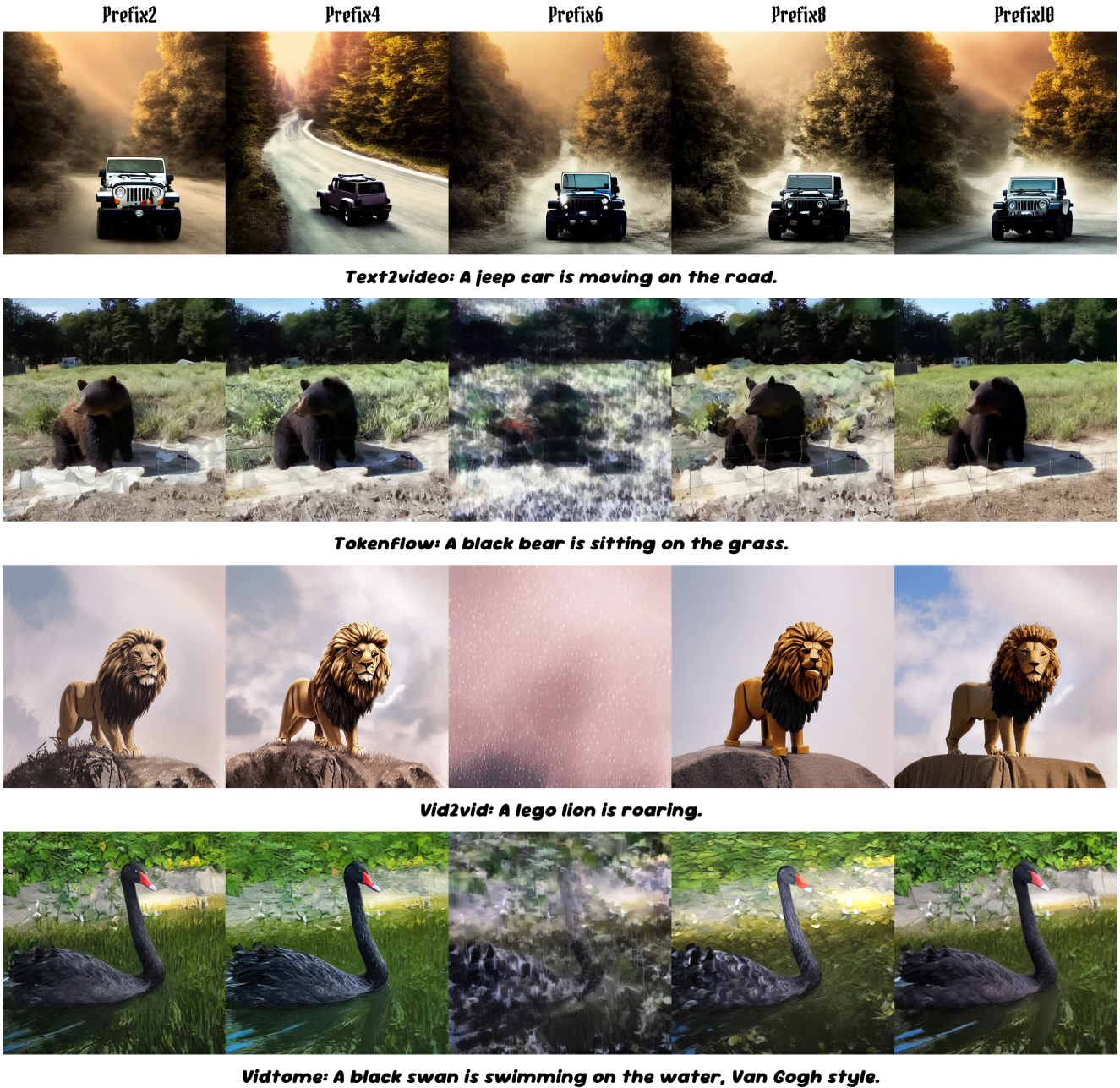


Figure 10: Visualization results obtained by Prompt learner taking different number of shared token (2, 4, 6, 8, 10) training and inference.

creating seamless biking dynamics and realistic water effects. Similarly, in the "walking dog" case, frame flickering and disjointed body movements are apparent without the adapter but are eliminated with its use, resulting in smooth, natural strides. Finally, in the "man surfing" example, the adapter improves semantic alignment, maintaining the surfer's balance and interaction with the waves, yielding visually coherent and dynamic transitions. These case studies demonstrate the adapter's effectiveness in achieving temporal stability, and semantic alignment, ensuring high-quality video outputs. In Figure 6 and Figure 7, we present a comparative analysis of the cross-attention maps generated by the stable diffusion base model and the modified model enhanced by our adapter during the image generation

process. Our observations indicate that subtle variations in the attention maps substantiate the impact of the adapter on the model's performance.

4.5. Ablation Study

Ablation of Token-Based Semantic Consistency Module.

Our ablation study demonstrates that shared tokens are critical for global semantic alignment, with the w Adapter model (integrating Shared Token and Adapter) significantly outperforming the Base model by ensuring consistent frame-level semantic focus on elements like the "swan" and "water" across timesteps, mitigating attention drift, enhancing fine-grained details like neck movements and water ripples, reducing irrelevant background attention, and facilitating smooth, cohesive transitions

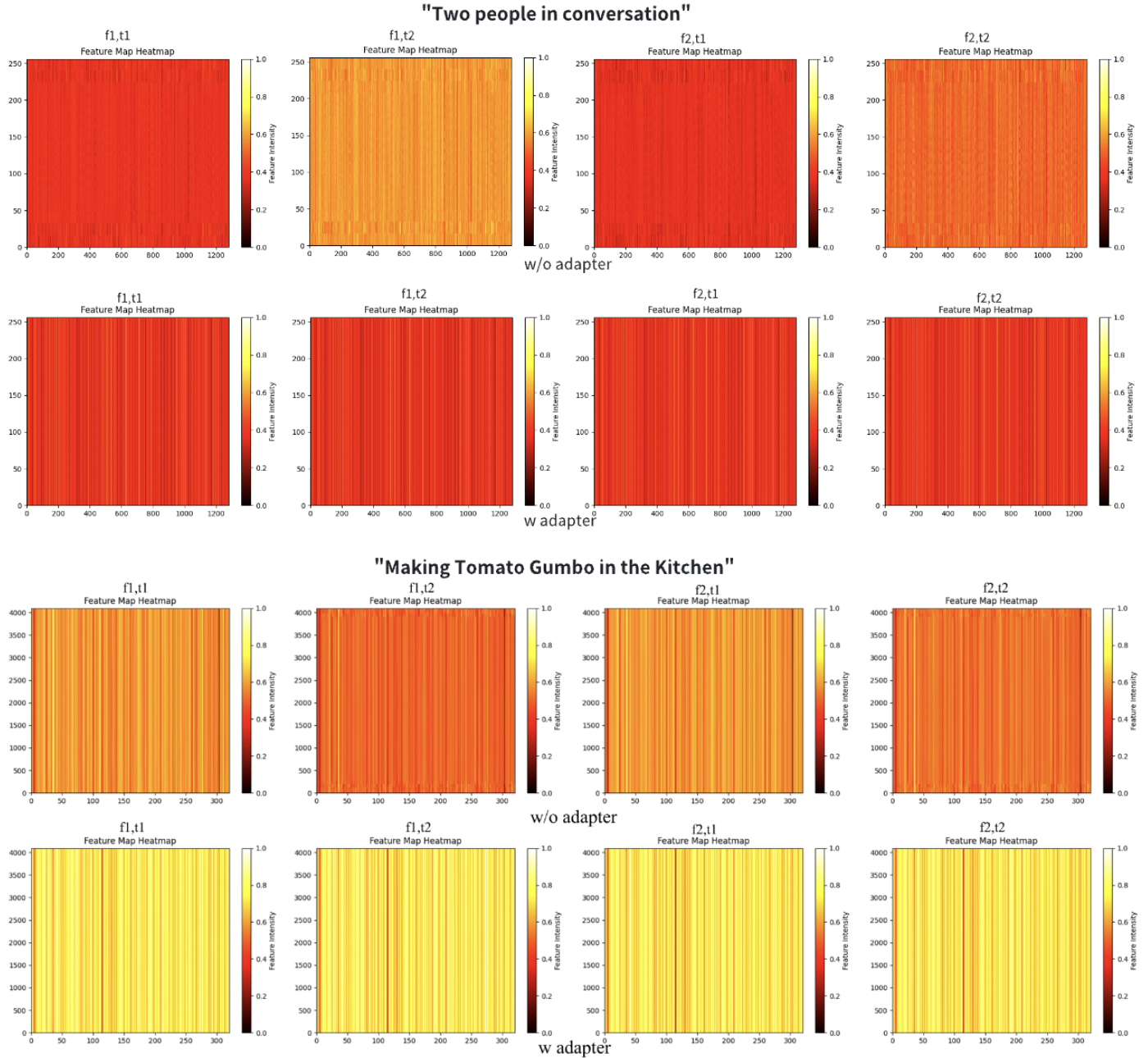


Figure 11: Comparison of single-channel feature heatmaps with and without adapter fine-tuning for scenarios 'Two People in Conversation' and 'Making Tomato Gumbo in the Kitchen,' showcasing features from the attention layer in UNet blocks 4-11. Labels f1/f2 denote adjacent frames, while t1/t2 represent timesteps (t1=932, t2=941) from the DDPM.

that integrate motion with ripple effects, showcasing superior semantic consistency and detailed representation. Removing shared tokens severely degrades semantic alignment, as shown in Figure 8, where TokenFlow's CLIP score drops from 29.4 to 20.1, FID increases from 135.7 to 387.8, and LPIPS rises from 0.14 to 0.17, disrupting global coherence and local detail quality, as further visualized in Figure 9, with the lion's shape and textures becoming unrecognizable.

The removal of shared tokens significantly hampers semantic consistency, as evident in examples like "A lion is roaring" and "A man is surfing" in Vid2Vid, where the generated outputs

lose alignment with the intended textual prompts. Similarly, for VidToMe, phrases like "A car is running" and "A child is riding" fail to maintain cohesion in the generated content, demonstrating a clear limitation when shared tokens are omitted.

Conversely, enhancing unshared tokens, while beneficial for maintaining original video attributes, poses its challenges. It often results in the model becoming overly dependent on the initial video content, reducing its adaptability to novel text-driven prompts. This limitation is evident in cases like "A lion is walking on the grass" in TokenFlow and "A man is running" in Text2Video, where the outputs struggle to effectively incorporate

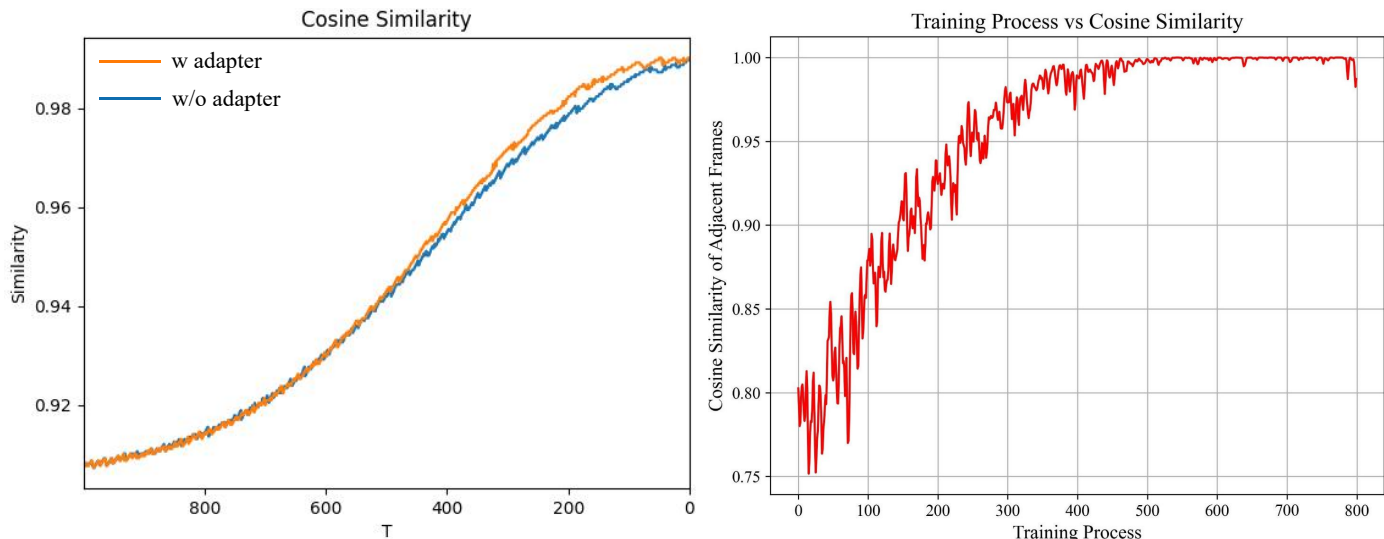


Figure 12: The left panel shows the average cosine similarity rise between interval framelatents during DDIM (the mean value is generated from the full training set of samples), the X-axis is the time step of DDIM, and the Y-axis is in units of 1, showing the consistency of the early noise with the adapter enabled. The right panel shows the jitter in similarity between adjacent frames during training, with the X-axis as the training epoch (1 epoch per 100 steps) and the Y-axis in units of 1, shows stability from 0 (no adapter) across training epochs as the adapter is enabled.

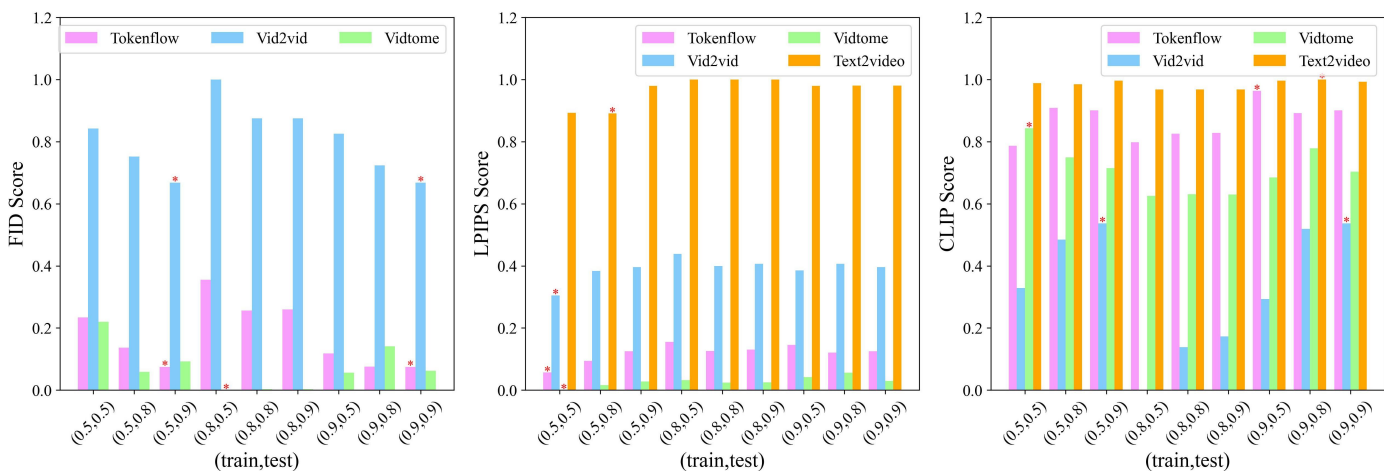


Figure 13: Bar chart illustrating the performance of four algorithms across three metrics for various combinations of (training timesteps, inference timesteps). The values 0.5, 0.8, and 0.9 represent the ranges 0.5t–1.0t, 0.8t–1.0t, and 0.9t–1.0t, respectively, where t denotes 1000 timesteps. The number on the left of the tuple indicates the training timesteps, while the number on the right represents the inference timesteps. Note that Text2Video, as a text-to-video generation algorithm, lacks pre-edited videos and therefore does not have an FID metric. The best (training timesteps, inference timesteps) combination for each algorithm is marked with an asterisk (*) at the top of the corresponding bar.

the textual input, indicating reduced flexibility in generating novel content.

Figures 8 and 9 highlight the critical need for balance, as excessive unshared tokens disrupt global semantic consistency and frame transitions, degrading all metrics, including TokenFlow’s CLIP score dropping to 27.8, FID increasing, and LPIPS worsening, underscoring the importance of integrating a well-balanced mix of shared and unshared tokens for both detail fidelity and global coherence. We also investigate the impact of the number of shared tokens in the Prompt Adapter on inference performance. In the main text, we analyze the resultant changes in metrics, and here we provide the relevant visualizations (refer to Figure 10).

Our findings support the hypothesis that an adequate number

of shared tokens enhances model performance across various algorithms. As the number of shared tokens increases, video quality stabilizes, and image details become smoother and richer. However, we observe that an excessive number of shared tokens may lead to the loss of textual information; for instance, a configuration with 18 shared tokens in vid2vid more effectively captures the Lego style compared to a configuration with 18 tokens. Consequently, we select 18 shared tokens as the optimal configuration for our final results.

Ablation of Multi-frame Latent Diffusion Model (Unet Adapter). This ablation study is to analyze the role of the Unet adapter in enhancing temporal consistency during video generation. Figure 11 highlights the critical impact of the Unet adapter on temporal feature consistency, as the feature map heatmaps re-

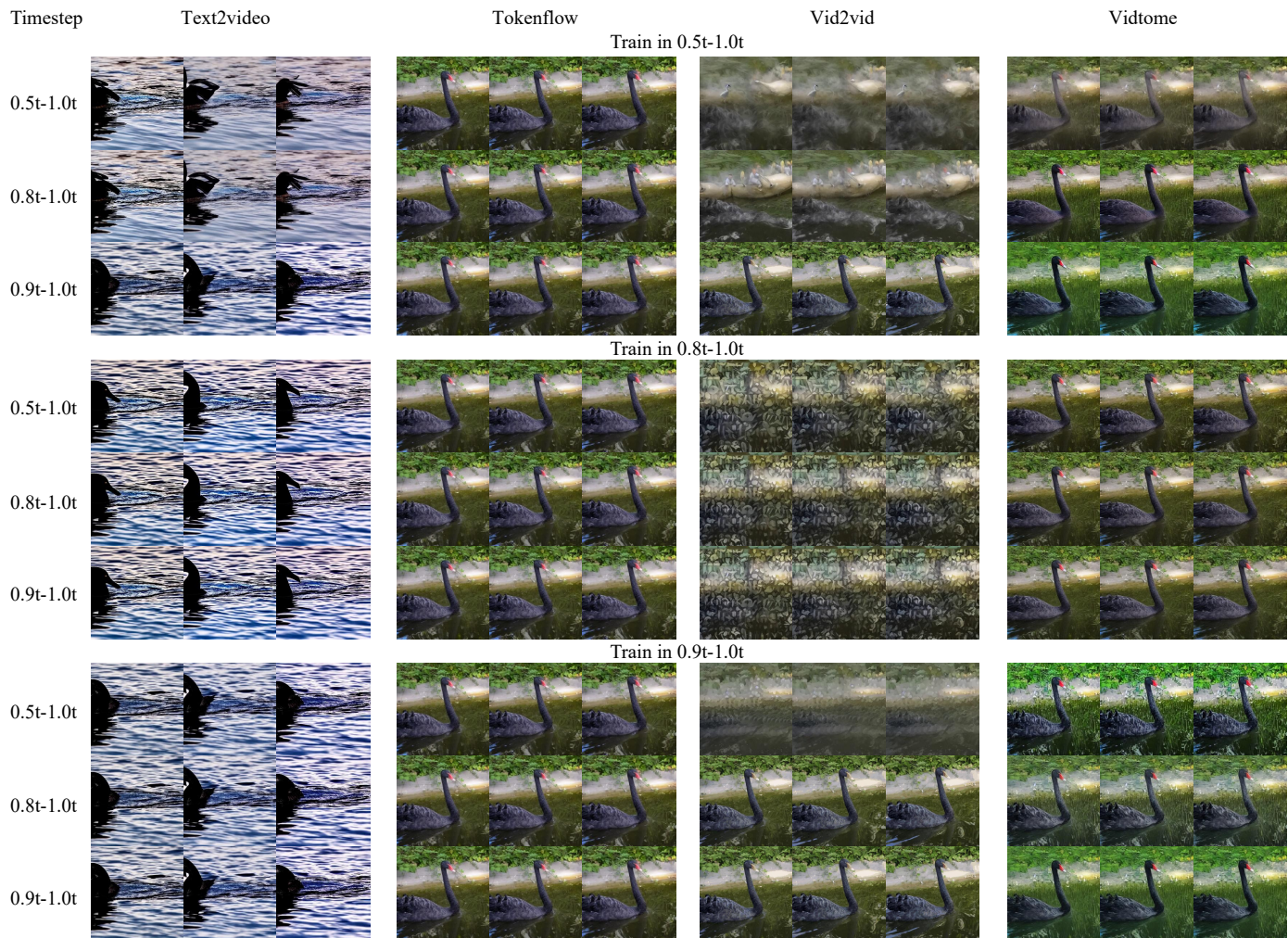


Figure 14: Visual comparison of a 0.5-1.0t training range for temporal-aware loss with a 0.9-1.0t adapter activation in inference range versus setting both to 0.5t ($t = 1000$).

veal stark contrasts between setups with and without the adapter. Without the adapter, inconsistencies such as structural disparities and reduced intensity alignment across adjacent frames (f_1, f_2) and timesteps (t_1, t_2) disrupt temporal transitions, leading to artifacts in video generation. This is further supported by the cosine similarity analysis in Figure 12, which evaluates the temporal coherence of the same video across different timesteps and adjacent frames during training. The left graph illustrates the average cosine similarity between frame embeddings at different timesteps within the same video, comparing models with and without adapter injection. Without the adapter, the similarity demonstrates slower growth and lower final values, indicating weaker temporal coherence. In contrast, the model with the adapter steadily improves, achieving higher cosine similarity and nearing 1.0, highlighting the adapter’s ability to enhance temporal consistency across timesteps.

The activation time period of the Unet adapter is crucial, as shown in Figure 13, which evaluates the effects of temporal-aware loss training ranges and adapter activation ranges during inference. While a 0.5-1.0 training range combined with a 0.5-1.0 inference range achieves the best metrics across CLIP,

FID, and LPIPS, Figure 14 reveals trade-offs: the broader 0.5-1.0 range introduces excessive constraints, resulting in over-smoothed details and visual blurriness. To resolve this, a narrower 0.9-1.0 inference range was adopted while keeping the broader 0.5-1.0 training range, striking a balance between temporal consistency and sharp, clear visual outputs.

Ablation of Hierarchical-Aware Temporal-Spatial Consistency Module This ablation study analyzes bilateral filtering in the Channel-Dependent Spatially Consistent Denoising Blocks. Figure 15 highlights the critical role of bilateral filtering in improving video quality. In the van, penguin, and rabbit cases, bilateral filtering produces smoother motion and clearer transitions between frames, eliminating the blurred edges and jitter seen without it. For the penguin, the waddling motion becomes more fluid and seamless, while the rabbit’s fur retains natural texture, with consistent motion transitions between jumps, free from artifacts. These visual improvements are supported by the quantitative data in Table 3, where TokenFlow with bilateral inversion shows a decrease in FID from 135.66 to 122.52, a slight increase in CLIP from 29.17 to 29.35, and a reduction in LPIPS from 0.142 to 0.136, confirming that bilateral filtering

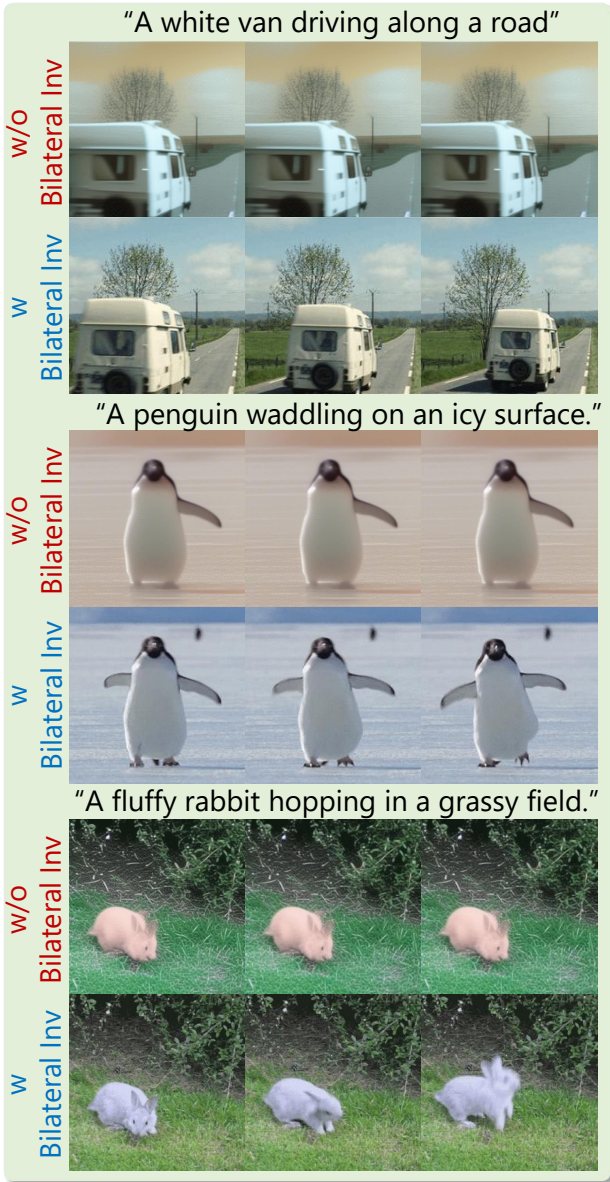


Figure 15: Comparison of video generation results with bilateral filtering using different kernel sizes in the Stable Diffusion pipeline.

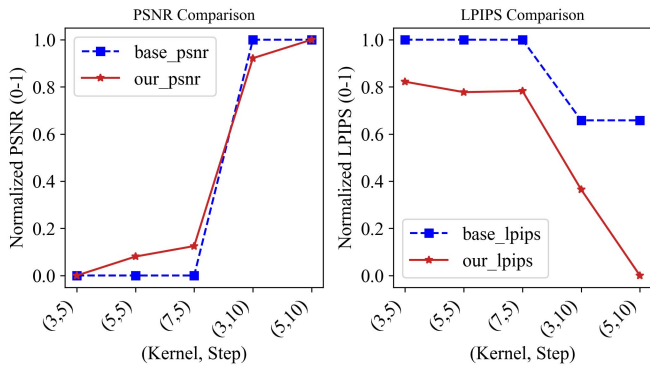


Figure 16: Comparison of step and kernel sizes $N(\cdot)$ within bilateral filtering inversion in the Stable Diffusion pipeline. The observed trends are consistent with those in vid2vid and three other algorithms (not shown due to space limitations).

enhances perceptual quality by reducing noise and improving image consistency.

We also explored the advantages of our inversion method at smaller step sizes, as shown in Figure 16, particularly in the 3-5 step configuration. At these smaller step sizes, our inversion method significantly improves temporal coherence, resulting in smoother transitions between frames. This is especially crucial in video generation, where smaller step sizes reduce noise and enhance fine details by minimizing artifacts like flickering or blurry transitions that often occur at larger step sizes. As a result, the model demonstrates more accurate frame-to-frame consistency, with enhanced details and smoother motion, underscoring the effectiveness of our inversion method at smaller step sizes.

Furthermore, as is shown in Figure 16, we also observed that by appropriately increasing the kernel size (and its corresponding steps), image quality metrics (e.g., PSNR) can be enhanced while simultaneously improving coherence (e.g., LPIPS), ultimately producing clearer and more coherent visual outputs.

Table 3: Ablation Study: Effects of Inv on Different Algorithms.

Algorithm	Bilateral Inv	FID ↓	CLIP ↑	LPIPS ↓
Tokenflow	✗	135.66	29.17	0.142
	✓	122.52	29.35	0.136
Vid2Vid	✗	387.76	20.08	0.210
	✓	320.80	25.84	0.166
VidToMe	✗	357.25	25.00	0.126
	✓	143.72	28.12	0.114
Text2Video	✗	–	29.10	0.347
	✓	–	30.07	0.244

4.6. User Study

We selected 67 random participants with diverse genders, ages, and educational backgrounds. They were asked to evaluate video outputs based on three dimensions: the coherence between frames, the alignment between text and frames, and the quality of the video frames themselves. For each algorithm, we selected 10 video editing cases with an adapter and 10 without, forming 20 pairs of videos in total. Each pair included one video generated with the adapter and one without. The participants were unaware of which videos had the adapter applied and were informed only that the videos were generated using different algorithms. They were instructed to choose the video they considered the best in each pair. Afterward, we collected their preferences for videos with and without adapters across all four algorithms, along with their selections in the three evaluation dimensions of text-to-image alignment, image quality, and consistency. Finally, we averaged the data from the 67 participants to calculate overall preference proportions for each algorithm and evaluation dimension. Figure 17 shows adapter-enhanced videos preferred across algorithms, with notable gains in consistency for VidToMe and image quality for TokenFlow, enhancing overall alignment and frame quality.

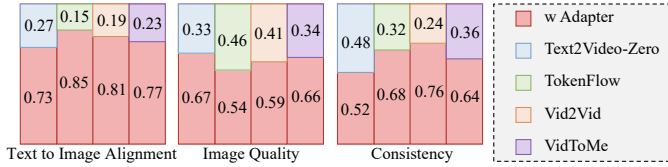


Figure 17: User study comparison of video generation algorithms with and without adding our adapter.

5. Conclusion and Future Work

To enhance temporal consistency and visual quality in video editing, we presented a prompt-learning adaptor leveraging pre-trained text-to-image diffusion models. We provide a plug-and-play solution that reduces flickering and improves text-to-image alignment, integrating seamlessly into existing workflows. The adaptor combines temporal-aware fine-tuning with a shared/unshared token mechanism to deliver significant improvements in both temporal consistency and video quality at low training costs. This application is compatible with a variety of video editing systems, providing a scalable and efficient alternative to text-driven video editing tools.

Limitations: Although the proposed adapter framework achieves significant improvements in temporal consistency, visual quality, and semantic alignment across different algorithms, it still has some limitations: its adaptability to complex prompts (e.g., significant changes to primary objects) is limited; improvements are less noticeable in cases without obvious flickering; in complex semantic scenarios, the minimal parameters make precise improvements challenging; while the shared token strategy ensures global consistency, it restricts frame-level flexibility; there are occasional discrepancies between quantitative metrics and visual outcomes; and scalability to complex video structures or high-resolution content remains insufficient.

Future work: Future work will enhance adaptability to complex prompts, improve subtle case performance, address complex semantics through parameter optimization and advanced architectures, refine token strategies for consistency and flexibility, align metrics with visual quality, enhance scalability for complex and high-resolution videos, explore adaptive temporal-aware fine-tuning, test diverse algorithms, and develop a generalized, personalized adapter with optimized speed, performance, and visual output for broader applicability and superior user experience.

Acknowledgment

This work is partially supported by Shenzhen Fundamental Research (General Program)(WDZC20231129163533001) and Hunan Provincial Transportation Science and Technology Project (No.202403).

References

Balaji, Y., Nah, S., Huang, X., Vahdat, A., Song, J., Zhang, Q., Kreis, K., Aittala, M., Aila, T., Laine, S., Catanzaro, B., Karras, T., and Liu, M.-Y. (2023). ediff-i: Text-to-image diffusion models with an ensemble of expert denoisers.

Bar-Tal, O., Chefer, H., Tov, O., Herrmann, C., Paiss, R., Zada, S., Ephrat, A., Hur, J., Liu, G., Raj, A., Li, Y., Rubinstein, M., Michaeli, T., Wang, O., Sun, D., Dekel, T., and Mosseri, I. (2024). Lumiere: A space-time diffusion model for video generation.

Cao, M., Wang, X., Qi, Z., Shan, Y., Qie, X., and Zheng, Y. (2023). Masactrl: Tuning-free mutual self-attention control for consistent image synthesis and editing.

Ceylan, D., Huang, C.-H. P., and Mitra, N. J. (2023). Pix2video: Video editing using image diffusion. In *Proceedings of the IEEE/CVF International Conference on Computer Vision*, pages 23206–23217.

Chai, W., Guo, X., Wang, G., and Lu, Y. (2023). Stablevideo: Text-driven consistency-aware diffusion video editing. In *Proceedings of the IEEE/CVF International Conference on Computer Vision*, pages 23040–23050.

Chen, Z., Duan, Y., Wang, W., He, J., Lu, T., Dai, J., and Qiao, Y. (2023). Vision transformer adapter for dense predictions.

Chu, E., Huang, T., Lin, S.-Y., and Chen, J.-C. (2024). Medm: Mediating image diffusion models for video-to-video translation with temporal correspondence guidance. In *Proceedings of the AAAI Conference on Artificial Intelligence*, volume 38, pages 1353–1361.

Cong, Y., Xu, M., Simon, C., Chen, S., Ren, J., Xie, Y., Perez-Rua, J.-M., Rosenhahn, B., Xiang, T., and He, S. (2023). Flatten: optical flow-guided attention for consistent text-to-video editing. *arXiv preprint arXiv:2310.05922*.

Devlin, J., Chang, M.-W., Lee, K., and Toutanova, K. (2019). Bert: Pre-training of deep bidirectional transformers for language understanding.

Feng, W., He, X., Fu, T.-J., Jampani, V., Akula, A., Narayana, P., Basu, S., Wang, X. E., and Wang, W. Y. (2023). Training-free structured diffusion guidance for compositional text-to-image synthesis.

Gao, B., Ren, J., Shen, F., Wei, M., and Huang, Z. (2024). Exploring warping-guided features via adaptive latent diffusion model for virtual try-on. In *2024 IEEE International Conference on Multimedia and Expo (ICME)*, pages 1–6. IEEE.

Garibi, D., Patashnik, O., Voynov, A., Averbuch-Elor, H., and Cohen-Or, D. (2024). Renoise: Real image inversion through iterative noising.

Geyer, M., Bar-Tal, O., Bagon, S., and Dekel, T. (2023a). Tokenflow: Consistent diffusion features for consistent video editing. *arXiv preprint arXiv:2307.10373*.

Geyer, M., Bar-Tal, O., Bagon, S., and Dekel, T. (2023b). Tokenflow: Consistent diffusion features for consistent video editing. *arXiv preprint arXiv:2307.10373*.

Geyer, M., Bar-Tal, O., Bagon, S., and Dekel, T. (2023c). Tokenflow: Consistent diffusion features for consistent video editing.

Guo, Y., Yang, C., Rao, A., Liang, Z., Wang, Y., Qiao, Y., Agrawala, M., Lin, D., and Dai, B. (2023). Animatediff: Animate your personalized text-to-image diffusion models without specific tuning. *arXiv preprint arXiv:2307.04725*.

Hong, W., Ding, M., Zheng, W., Liu, X., and Tang, J. (2022). Cogvideo: Large-scale pretraining for text-to-video generation via transformers. *arXiv preprint arXiv:2205.15868*.

Houlsby, N., Giurgiu, A., Jastrzebski, S., Morrone, B., de Laroussilhe, Q., Gesmundo, A., Attariyan, M., and Gelly, S. (2019). Parameter-efficient transfer learning for nlp.

Huo, J., Wang, Z., Zhao, R., Sun, L., and Shen, F. (2024). Synthesizing high-quality construction segmentation datasets through pre-trained diffusion model. In *International Conference on Intelligent Computing*, pages 354–366. Springer.

Kang, W., Galim, K., and Koo, H. I. (2024). Eta inversion: Designing an optimal eta function for diffusion-based real image editing.

Karras, T., Aittala, M., Laine, S., Härkönen, E., Hellsten, J., Lehtinen, J., and Aila, T. (2021). Alias-free generative adversarial networks. In Ranzato, M., Beygelzimer, A., Dauphin, Y., Liang, P., and Vaughan, J. W., editors, *Advances in Neural Information Processing Systems*, volume 34, pages 852–863. Curran Associates, Inc.

Karras, T., Laine, S., Aittala, M., Hellsten, J., Lehtinen, J., and Aila, T. (2020). Analyzing and improving the image quality of stylegan. In *Proceedings of the IEEE/CVF Conference on Computer Vision and Pattern Recognition (CVPR)*.

Khachatryan, L., Movsisyan, A., Tadevosyan, V., Henschel, R., Wang, Z., Navasardyan, S., and Shi, H. (2023). Text2video-zero: Text-to-image diffusion models are zero-shot video generators.

Kim, J. and Kim, T.-K. (2024). Arbitrary-scale image generation and upsampling using latent diffusion model and implicit neural decoder. In *Proceedings of the IEEE/CVF Conference on Computer Vision and Pattern Recognition*, pages 9202–9211.

- Li, X., Ma, C., Yang, X., and Yang, M.-H. (2023). Vidtope: Video token merging for zero-shot video editing.
- Liu, J., Huang, H., Jin, C., and He, R. (2023). Portrait diffusion: Training-free face stylization with chain-of-painting.
- Liu, Y., Zhang, K., Li, Y., Yan, Z., Gao, C., Chen, R., Yuan, Z., Huang, Y., Sun, H., Gao, J., He, L., and Sun, L. (2024). Sora: A review on background, technology, limitations, and opportunities of large vision models.
- Lu, C., Zhou, Y., Bao, F., Chen, J., Li, C., and Zhu, J. (2022). Dpm-solver: A fast ode solver for diffusion probabilistic model sampling in around 10 steps. *Advances in Neural Information Processing Systems*, 35:5775–5787.
- Mou, C., Wang, X., Xie, L., Wu, Y., Zhang, J., Qi, Z., Shan, Y., and Qie, X. (2023). T2i-adapter: Learning adapters to dig out more controllable ability for text-to-image diffusion models.
- Pan, Y., Qiu, Z., Yao, T., Li, H., and Mei, T. (2018). To create what you tell: Generating videos from captions.
- Qi, T., Fang, S., Wu, Y., Xie, H., Liu, J., Chen, L., He, Q., and Zhang, Y. (2024). Deadiff: An efficient stylization diffusion model with disentangled representations.
- Qian, Q., Xu, H., Yan, M., and Hu, J. (2024). Siminversion: A simple framework for inversion-based text-to-image editing.
- Radford, A. (2018). Improving language understanding by generative pre-training. Technical report, OpenAI. OpenAI technical report.
- Ren, Y., Zhou, Y., Yang, J., Shi, J., Liu, D., Liu, F., Kwon, M., and Shrivastava, A. (2024). Customize-a-video: One-shot motion customization of text-to-video diffusion models.
- Rombach, R., Blattmann, A., Lorenz, D., Esser, P., and Ommer, B. (2022). High-resolution image synthesis with latent diffusion models. In *Proceedings of the IEEE/CVF conference on computer vision and pattern recognition*, pages 10684–10695.
- Salimans, T. and Ho, J. (2022). Progressive distillation for fast sampling of diffusion models. *arXiv preprint arXiv:2202.00512*.
- Sauer, A., Schwarz, K., and Geiger, A. (2022). Stylegan-xl: Scaling stylegan to large diverse datasets.
- Shen, F., Jiang, X., He, X., Ye, H., Wang, C., Du, X., Li, Z., and Tang, J. (2024a). Imagdressing-v1: Customizable virtual dressing. *arXiv preprint arXiv:2407.12705*.
- Shen, F., Shu, X., Du, X., and Tang, J. (2023a). Pedestrian-specific bipartite-aware similarity learning for text-based person retrieval. In *Proceedings of the 31th ACM International Conference on Multimedia*.
- Shen, F. and Tang, J. (2024). Imagpose: A unified conditional framework for pose-guided person generation. In *The Thirty-eighth Annual Conference on Neural Information Processing Systems*.
- Shen, F., Xie, Y., Zhu, J., Zhu, X., and Zeng, H. (2023b). Git: Graph interactive transformer for vehicle re-identification. *IEEE Transactions on Image Processing*.
- Shen, F., Ye, H., Liu, S., Zhang, J., Wang, C., Han, X., and Yang, W. (2024b). Boosting consistency in story visualization with rich-contextual conditional diffusion models. *arXiv preprint arXiv:2407.02482*.
- Shen, F., Ye, H., Zhang, J., Wang, C., Han, X., and Yang, W. (2023c). Advancing pose-guided image synthesis with progressive conditional diffusion models. *arXiv preprint arXiv:2310.06313*.
- Singer, U., Polyak, A., Hayes, T., Yin, X., An, J., Zhang, S., Hu, Q., Yang, H., Ashual, O., Gafni, O., Parikh, D., Gupta, S., and Taigman, Y. (2022). Make-a-video: Text-to-video generation without text-video data.
- Song, J., Meng, C., and Ermon, S. (2022). Denoising diffusion implicit models.
- Soviany, P., Ardei, C., Ionescu, R. T., and Leordeanu, M. (2019). Image difficulty curriculum for generative adversarial networks (cugan).
- Wang, C., Tian, K., Guan, Y., Zhang, J., Jiang, Z., Shen, F., Han, X., Gu, Q., and Yang, W. (2024a). Ensembling diffusion models via adaptive feature aggregation. *arXiv preprint arXiv:2405.17082*.
- Wang, C., Tian, K., Zhang, J., Guan, Y., Luo, F., Shen, F., Jiang, Z., Gu, Q., Han, X., and Yang, W. (2024b). V-express: Conditional dropout for progressive training of portrait video generation. *arXiv preprint arXiv:2406.02511*.
- Wang, F.-Y., Chen, W., Song, G., Ye, H.-J., Liu, Y., and Li, H. (2023a). Genl-video: Multi-text to long video generation via temporal co-denoising. *arXiv preprint arXiv:2305.18264*.
- Wang, J., Yuan, H., Chen, D., Zhang, Y., Wang, X., and Zhang, S. (2023b). Modelscope text-to-video technical report.
- Wang, T.-C., Liu, M.-Y., Zhu, J.-Y., Liu, G., Tao, A., Kautz, J., and Catanzaro, B. (2018). Video-to-video synthesis.
- Wang, W., Jiang, Y., Xie, K., Liu, Z., Chen, H., Cao, Y., Wang, X., and Shen, C. (2023c). Zero-shot video editing using off-the-shelf image diffusion models. *arXiv e-prints*, pages arXiv–2303.
- Wang, X., Zhang, S., Yuan, H., Qing, Z., Gong, B., Zhang, Y., Shen, Y., Gao, C., and Sang, N. (2024c). A recipe for scaling up text-to-video generation with text-free videos. In *Proceedings of the IEEE/CVF Conference on Computer Vision and Pattern Recognition*, pages 6572–6582.
- Wu, J. Z., Ge, Y., Wang, X., Lei, W., Gu, Y., Shi, Y., Hsu, W., Shan, Y., Qie, X., and Shou, M. Z. (2023a). Tune-a-video: One-shot tuning of image diffusion models for text-to-video generation.
- Wu, J. Z., Ge, Y., Wang, X., Lei, W., Gu, Y., Shi, Y., Hsu, W., Shan, Y., Qie, X., and Shou, M. Z. (2023b). Tune-a-video: One-shot tuning of image diffusion models for text-to-video generation.
- Xu, J., Mei, T., Yao, T., and Rui, Y. (2016). Msr-vtt: A large video description dataset for bridging video and language. In *2016 IEEE Conference on Computer Vision and Pattern Recognition (CVPR)*, pages 5288–5296.
- Xu, R., Shen, F., Xie, X., and Li, Z. (2024). Training-free diffusion models for content-style synthesis. In *International Conference on Intelligent Computing*, pages 308–319. Springer.
- Yan, H., Liew, J. H., Mai, L., Lin, S., and Feng, J. (2023). Magicprop: Diffusion-based video editing via motion-aware appearance propagation. *arXiv preprint arXiv:2309.00908*.
- Yan, W., Zhang, Y., Abbeel, P., and Srinivas, A. (2021). Videogpt: Video generation using vq-vae and transformers. *arXiv preprint arXiv:2104.10157*.
- Zhang, L., Rao, A., and Agrawala, M. (2023). Adding conditional control to text-to-image diffusion models.
- Zhang, Z., Lin, M., Yan, S., and Ji, R. (2024). Easyinv: Toward fast and better ddim inversion.
- Zhao, M., Wang, R., Bao, F., Li, C., and Zhu, J. (2023a). Controlvideo: Adding conditional control for one shot text-to-video editing. *arXiv preprint arXiv:2305.17098*, 2(3).
- Zhao, S., Chen, D., Chen, Y.-C., Bao, J., Hao, S., Yuan, L., and Wong, K.-Y. K. (2023b). Uni-controlnet: All-in-one control to text-to-image diffusion models.